

**Hygroscopic  
properties of  
 $\text{Ca}(\text{NO}_3)_2$  particles by  
Raman spectra**

Y. J. Liu et al.

**Investigation of the hygroscopic  
properties of  $\text{Ca}(\text{NO}_3)_2$  and internally  
mixed  $\text{Ca}(\text{NO}_3)_2/\text{CaCO}_3$  particles by  
micro-Raman spectrometry**

Y. J. Liu, T. Zhu, D. F. Zhao, and Z. F. Zhang

State Key Joint Laboratory of Environmental Simulation and Pollution Control, School of  
Environmental Science and Engineering, Peking University, Beijing 100871, China

Received: 9 April 2008 – Accepted: 28 April 2008 – Published: 3 June 2008

Correspondence to: T. Zhu (tzhu@pku.edu.cn)

Published by Copernicus Publications on behalf of the European Geosciences Union.

Title Page

Abstract

Introduction

Conclusions

References

Tables

Figures

⏪

⏩

◀

▶

Back

Close

Full Screen / Esc

Printer-friendly Version

Interactive Discussion

## Abstract

To understand and predict the role of mineral aerosol particles processed by reactive nitrogen species in the atmosphere, the hygroscopic properties of both  $\text{Ca}(\text{NO}_3)_2$  and  $\text{Ca}(\text{NO}_3)_2$ -containing mineral particles must be well understood. Using a micro-Raman system, the dehydration and hydration processes of micro-sized individual  $\text{Ca}(\text{NO}_3)_2$  and internally mixed  $\text{Ca}(\text{NO}_3)_2/\text{CaCO}_3$  particles were investigated systematically. In addition to accurate quantification of the dependence of water content on relative humidity (RH), significant new spectroscopic evidence related to chemical structure was also obtained to confirm the occurrence of amorphous solid state and to better understand the phase transition process. The  $\text{Ca}(\text{NO}_3)_2$  particles exhibit reversible behavior in the dehydration and hydration processes; they are in the state of solution droplets above 10% RH and amorphous hydrates below 7% RH, and phase transition occurs at 7–10% RH. The hygroscopic behavior of  $\text{Ca}(\text{NO}_3)_2/\text{CaCO}_3$  particles is identical to that of pure  $\text{Ca}(\text{NO}_3)_2$  particles, suggesting a negligible effect of the inclusion of slightly soluble  $\text{CaCO}_3$ .

## 1 Introduction

Large quantities of mineral dust particles are emitted from desert and arid regions on the earth every year (Tegen et al., 1996) and transported over long distances, influencing the climate and atmospheric chemistry on both regional and global scales (Dentener et al., 1996; Seinfeld et al., 2004; Tang et al., 2004). When transported through a polluted atmosphere, reactive components of mineral aerosols such as calcite and dolomite can react readily with reactive nitrogen species to yield nitrate salt products (Song and Carmichael, 2001; Krueger et al., 2003, 2004). The presence of  $\text{Ca}(\text{NO}_3)_2$  in aged mineral aerosols has been verified by single-particle analysis in different areas of the world (Lee et al., 2002; Mamane and Gottlieb, 1992; Ro et al., 2005). Recently, it has been confirmed that  $\text{CaCO}_3$  dust particles in the atmosphere

## Hygroscopic properties of $\text{Ca}(\text{NO}_3)_2$ particles by Raman spectra

Y. J. Liu et al.

Title Page

Abstract

Introduction

Conclusions

References

Tables

Figures

⏪

⏩

◀

▶

Back

Close

Full Screen / Esc

Printer-friendly Version

Interactive Discussion

can be converted completely to  $\text{Ca}(\text{NO}_3)_2$  (Laskin et al., 2005a; Sullivan et al., 2007). In comparison to carbonate minerals, the  $\text{Ca}(\text{NO}_3)_2$  product is very soluble and should have very different hygroscopic behavior. Because phase and water content govern the shape, size, refractive index, and reactivity of aerosol particles, the hygroscopic properties of both  $\text{Ca}(\text{NO}_3)_2$  particles and  $\text{Ca}(\text{NO}_3)_2$ -containing mineral particles should be investigated in detail before evaluating the effect of mineral dust particles on climate and atmospheric chemistry.

The hygroscopic behavior of  $\text{Ca}(\text{NO}_3)_2$  particles has been investigated in laboratory studies using the electrodynamic balance (EDB; Tang and Fung, 1997), environmental scanning electron microscope (ESEM; Laskin et al., 2005b), and tandem differential mobility analyzer (TDMA; Gibson et al., 2006). Whereas the EDB measurements covered both dehydration and hydration processes, the other two studies focused only on the hydration process. Although all three studies agreed that deliquescence transition of  $\text{Ca}(\text{NO}_3)_2$  particles occurred between solution phase and amorphous solid phase that has not been observed previously in bulk samples, only Tang and Fung attempted to describe the amorphous phase in terms of water content and morphological features. Moreover, the deliquescence transition process did not show good agreement among the three studies. EDB measurements indicated that the particle water content increased from 10% relative humidity (RH) and reached that of the corresponding supersaturated droplets at 15% RH. Using ESEM, Laskin et al. (2005b) observed initial morphological changes at 8% RH, a further volume increase at 9–10% RH, and fully developed droplet formation at 11% RH. Because only a very small change in size was measured, the TDMA study concluded that the transition occurred close to 10% RH.

The investigation of the hygroscopic properties of  $\text{Ca}(\text{NO}_3)_2$ -containing mineral particles has been limited to ESEM observations. Laskin et al. (2005b) reported that individual  $\text{Ca}(\text{NO}_3)_2$  particles and internally mixed  $\text{Ca}(\text{NO}_3)_2/\text{CaCO}_3$  particles showed identical morphological changes from 7 to 11% RH, suggesting similar deliquescence processes. Shi et al. (2008) observed  $\text{Ca}(\text{NO}_3)_2$ -containing dust particles in the aqueous phase at 15% RH, which increased in size with increasing humidity. There have been

## Hygroscopic properties of $\text{Ca}(\text{NO}_3)_2$ particles by Raman spectra

Y. J. Liu et al.

Title Page

Abstract

Introduction

Conclusions

References

Tables

Figures

⏪

⏩

◀

▶

Back

Close

Full Screen / Esc

Printer-friendly Version

Interactive Discussion

no more systematic investigations of the hygroscopic behavior of  $\text{Ca}(\text{NO}_3)_2$ -containing mineral dust particles, including both deliquescence and efflorescence transition and the RH dependence of the water content.

Micro-Raman spectroscopy allows in situ analyses of the dynamic processes of micro-sized individual aerosol particles and has unexplored potential in characterizing aerosol hygroscopic behavior. The concentration dependence of spontaneous Raman scattering allows the quantitative analysis of the water content of liquid droplets (Reid et al., 2007), at the same time, peak position of the anion Raman band is a sensitive indicator of the chemical structure of particles and hence phase transition (Widmann et al., 1998; Musick et al., 2000). Moreover, morphological changes can also be observed with microscope equipped to Raman spectrometer. It should be noted that micro-Raman spectrometry was combined with EDB in Tang and Fung's (1997) study of  $\text{Ca}(\text{NO}_3)_2$  particles, but has been used mainly to study ion associations and hydrogen bonds in concentrated solution, rather than to characterize phase transition and hygroscopic growth.

We used micro-Raman spectrometry as a standalone technique to investigate the hygroscopic behavior of micro-sized particles deposited on fluorinated ethylene propylene (FEP) substrate. Both pure  $\text{Ca}(\text{NO}_3)_2$  particles and internally mixed  $\text{Ca}(\text{NO}_3)_2/\text{CaCO}_3$  particles were studied. The particle water content was quantified using the intensity ratio of the water band to the solute band, and new spectroscopic evidences related to structural changes were provided for phase transition and phase determination. We present the hygroscopic behavior measurements and compare them with those of previous studies and bulk thermodynamic predictions.

## Hygroscopic properties of $\text{Ca}(\text{NO}_3)_2$ particles by Raman spectra

Y. J. Liu et al.

Title Page

Abstract

Introduction

Conclusions

References

Tables

Figures

⏪

⏩

◀

▶

Back

Close

Full Screen / Esc

Printer-friendly Version

Interactive Discussion

## 2 Experimental

### 2.1 Apparatus and procedures

The experimental setup and sample cell are illustrated in Fig. 1. The sample cell was designed with reference to the reaction cell used to study the heterogeneous reactions of individual particles by Raman spectrometry (Chen et al., 2005) and the flow cell used to study the deliquescence of organic acid particles by optical microscopy (Parsons et al., 2004). The lid and body of the cell were constructed of stainless steel. A piece of round cover glass (25 mm in diameter, 0.15 mm thick) was used as the top window and was sealed to the cell lid with high vacuum grease. The cell lid was sealed to the cell body using a fluororubber O-ring. Substrate carrying individual particles was fixed on the sample holder.

An ideal substrate for the characterization of individual aerosol particles by micro-Raman spectrometry was considered to have a flat stable surface, lack of Raman response, tolerance for high laser densities, and ease of particle recognition (Godoi et al., 2006). For the investigation of particle hygroscopic behavior, the substrate should also be strongly hydrophobic so that heterogeneous nucleation of the droplets on the substrate can be suppressed. Thus, we used 0.1 mm thick Teflon<sup>®</sup> FEP film (DuPont) as the substrate. Its strengths include: (1) high chemical inertness and stability to laser radiation; (2) strong hydrophobic properties and a very flat surface after annealing; (3) relatively low Raman signals, no overlap with the strong  $\nu_1$ -NO<sub>3</sub><sup>-</sup> band and the OH stretching vibration envelope; (4) many sharp Raman lines providing good internal standards for the spectra calibration of aerosol particles; and (5) high contrast to particles on it as a substrate, thus facilitating microscopic observation. Of course, the FEP film has some limitations: its  $\nu_1$ (CF<sub>2</sub>) band at 734 cm<sup>-1</sup> overlaps with some weak bands of salts of interest such as  $\nu_4$ -NO<sub>3</sub><sup>-</sup>, which is sensitive to contact ion pairs in supersaturated droplets.

Before use, the FEP film was annealed to a silicon wafer for ease of manipulation

## Hygroscopic properties of Ca(NO<sub>3</sub>)<sub>2</sub> particles by Raman spectra

Y. J. Liu et al.

Title Page

Abstract

Introduction

Conclusions

References

Tables

Figures

⏪

⏩

◀

▶

Back

Close

Full Screen / Esc

Printer-friendly Version

Interactive Discussion

with reference to the method of Parsons et al. (2004). The annealing process can significantly reduce the number of defects on the surface of the FEP film.

The relative humidity in the cell was regulated by the continuous flow of a mixture of dry and humidified N<sub>2</sub>. Ultra-high-purity nitrogen (99.999%, Beijing Huilong Changhai) was first passed through a liquid N<sub>2</sub> trap to remove impurities such as hydrocarbons and water vapor and was then split into two streams; one stream was humidified by bubbling through deionized water (18.2 MΩ·cm, Milli-Q, Millipore) and was then mixed with the other stream. The relative humidity in the sample cell was varied by adjusting the ratio of the flow rates of dry and humidified N<sub>2</sub> using mass flow controllers while maintaining a total flow rate of 200 ml/min. Internally mixed Ca(NO<sub>3</sub>)<sub>2</sub>/CaCO<sub>3</sub> particles was prepared by exposing individual CaCO<sub>3</sub> particles to NO<sub>2</sub>/H<sub>2</sub>O/N<sub>2</sub> mixture, which was generated by adding the third stream of NO<sub>2</sub> (2000 ppm; Messer) at a controlled flow rate. The relative humidity and temperature of the outflow from the sample cell were measured using a hygrometer (HMT 100; Vaisala) that had a measurement accuracy of ±1.7% RH and ±0.2°C. Because a temperature difference between the humidity sensor and the zone of interest will cause considerable error in RH measurement, the sample cell was equipped with another small temperature sensor (Pt 100, 1/3 DIN B; Heraeus) that had an accuracy of ±0.2°C. The distance from the temperature sensor to the substrate was <10 mm; thus, it was safe to take the measured value as the local temperature over the substrate. Because the absolute humidity of the gas stream was constant at equilibrium, the local RH over the substrate could be calculated using the known local temperature, outflow RH, and outflow temperature.

A commercially available micro-Raman spectrometer (LabRam HR 800; Horiba Jobin Yvon) was used. This spectrometer is equipped with a microscope (Olympus BX40), a motorized x, y-stage, and a charge-coupled device (CCD) detector. The sample cell was mounted on the x, y-stage. The excitation source was an argon ion laser (Spectra Physics) operating at 514.5 nm with an output power of 25 mW. A 50×NA0.5 long working distance objective was used. The excitation laser was focused through the top window of the sample cell onto the particle of interest. The backscattering sig-

---

## Hygroscopic properties of Ca(NO<sub>3</sub>)<sub>2</sub> particles by Raman spectra

Y. J. Liu et al.

---

Title Page

Abstract

Introduction

Conclusions

References

Tables

Figures

⏪

⏩

◀

▶

Back

Close

Full Screen / Esc

Printer-friendly Version

Interactive Discussion

---

**Hygroscopic properties of  $\text{Ca}(\text{NO}_3)_2$  particles by Raman spectra**

---

Y. J. Liu et al.

[Title Page](#)[Abstract](#)[Introduction](#)[Conclusions](#)[References](#)[Tables](#)[Figures](#)[⏪](#)[⏩](#)[◀](#)[▶](#)[Back](#)[Close](#)[Full Screen / Esc](#)[Printer-friendly Version](#)[Interactive Discussion](#)

nal, after passing through 600 g/mm grating, was detected by the CCD. Raman spectra in the range of 100–4000  $\text{cm}^{-1}$  were obtained using an exposure time of 10 s. The microscopic images of the particle of interest were also recorded to observe phase transition and morphological change. For  $\text{NO}_2$ -treated  $\text{CaCO}_3$  particles, Raman spectrum were collected over a  $12\ \mu\text{m} \times 12\ \mu\text{m}$  area using a step of  $2\ \mu\text{m}$  and an exposure time of 5 s. The intensity of Raman bands at  $\sim 1050\ \text{cm}^{-1}$  ( $\nu_1\text{-NO}_3^-$ ) and  $\sim 1085\ \text{cm}^{-1}$  ( $\nu_1\text{-CO}_3^{2-}$ ) were mapped to investigate the relative amount of each component.

The  $(\text{NH}_4)_2\text{SO}_4$  (99.999%; Alfa Aesar),  $\text{Ca}(\text{NO}_3)_2 \cdot 4\text{H}_2\text{O}$  (ACS, 99–103%; Riedel-de Haën), and  $\text{CaCO}_3$  (99.999%; Alfa Aesar) were used without further purification. All of the salts were ground and then dispersed on the substrate. Three to six individual particles with diameters of 5–10  $\mu\text{m}$  were selected for investigation in each experiment. During a typical experiment, the relative humidity was increased or decreased in steps of 1–20% RH. Smaller steps were used around phase transition points. Pre-experiments with different equilibrium times were performed to ensure that the particles could achieve the equilibrium state at each RH. All of the measurements were made at ambient temperatures of  $25 \pm 0.5^\circ\text{C}$ .

## 2.2 Quantification of particle water content

The concentration dependence of spontaneous Raman scattering allows the quantitative analysis of the water content of liquid droplets (Reid et al., 2007). Jordanov and Zellner (2006) attempted to quantify the RH dependence of water content in levitated  $(\text{NH}_4)_2\text{SO}_4$  particles with Raman spectroscopy, but were unsuccessful because of strong band distortion of  $\text{NH}_4^+$  and  $\text{H}_2\text{O}$  caused by the morphology-dependent resonances of spherical droplets. In contrast, the disturbance of morphology-dependent resonances was successfully excluded from our experiment by depositing particles on the substrate, rather than levitating them.

We quantified the water content of  $\text{Ca}(\text{NO}_3)_2$  droplets using the ratio of the integrated intensity of the  $\text{H}_2\text{O}$  stretching envelope ( $2900\text{--}3800\ \text{cm}^{-1}$ ) to that of  $\nu_1\text{-NO}_3^-$

## Hygroscopic properties of $\text{Ca}(\text{NO}_3)_2$ particles by Raman spectra

Y. J. Liu et al.

Title Page

Abstract

Introduction

Conclusions

References

Tables

Figures

◀

▶

◀

▶

Back

Close

Full Screen / Esc

Printer-friendly Version

Interactive Discussion



over  $1010\text{--}1090\text{ cm}^{-1}$ . For  $(\text{NH}_4)_2\text{SO}_4$  droplets, the stretching envelope of  $\text{NH}_4^+$  overlapped with that of  $\text{H}_2\text{O}$ ; hence, the total intensities of these two envelopes were integrated at first, then the water content of  $(\text{NH}_4)_2\text{SO}_4$  droplets can be calculated according to:

$$\frac{I_{\text{NH,OH}}}{I_{\text{Sulfate}}} = \frac{A \cdot n_{\text{H}_2\text{O}} + B \cdot n_{\text{NH}_4^+}}{C \cdot n_{\text{SO}_4^{2-}}} = \frac{A}{C} \cdot \frac{n_{\text{H}_2\text{O}}}{n_{\text{SO}_4^{2-}}} + \frac{2B}{C} \quad (1)$$

where  $I_{\text{NH,OH}}$  is the integrated intensity of the NH and OH stretching envelope over  $2680\text{--}3780\text{ cm}^{-1}$ ;  $I_{\text{Sulfate}}$  is the integrated intensity of  $\nu_1\text{-SO}_4^{2-}$  over  $940\text{--}1020\text{ cm}^{-1}$ ;  $n_{\text{H}_2\text{O}}$ ,  $n_{\text{NH}_4^+}$ , and  $n_{\text{SO}_4^{2-}}$  are the molecular numbers of  $\text{H}_2\text{O}$ ,  $\text{NH}_4^+$ , and  $\text{SO}_4^{2-}$  in the solution, respectively; and A, B, and C are constants.

A series of bulk solutions reaching the saturation point of each salt were prepared for calibration. Because the  $\text{Ca}(\text{NO}_3)_2$  solution can readily supersaturate even in the bulk phase (Stokes and Robinson, 1948), a supersaturated  $\text{Ca}(\text{NO}_3)_2$  bulk solution with a 4:1 molar ratio of  $\text{H}_2\text{O}$ : solute was prepared by cooling the melted  $\text{Ca}(\text{NO}_3)_2 \cdot 4\text{H}_2\text{O}$  crystals. The calibration curves of  $\text{Ca}(\text{NO}_3)_2$  and  $(\text{NH}_4)_2\text{SO}_4$  were extrapolated linearly to supersaturated concentrations (Appendix A).

### 2.3 Raman spectra treatment

The obtained Raman spectra were analyzed using Labspec 5 software. The  $\nu_1\text{-SO}_4^{2-}$  Raman band centered at  $\sim 978\text{ cm}^{-1}$  and the  $\nu_1\text{-NO}_3^-$  Raman band centered at  $\sim 1055\text{ cm}^{-1}$  were fit to the Gaussian-Lorentz function to obtain precise values of peak position and full width at half-maximum (FWHM).  $\text{CF}_2$  bend vibration of the FEP substrate at  $383\text{ cm}^{-1}$  (Hannon et al., 1969) was also fit and taken as an internal calibrator of peak position.

### 3 Results

#### 3.1 Hygroscopic properties of $(\text{NH}_4)_2\text{SO}_4$ particles

The hygroscopic properties of  $(\text{NH}_4)_2\text{SO}_4$  have been studied extensively and are well understood. To evaluate the performance of our experimental apparatus and approach, we first studied  $(\text{NH}_4)_2\text{SO}_4$  particles. Figure 2 shows the RH dependence of the water content of  $(\text{NH}_4)_2\text{SO}_4$  in hydration and dehydration processes. The quantified water-to-solute molar ratio (WSR) of  $(\text{NH}_4)_2\text{SO}_4$  droplets showed excellent agreement with that measured by Tang and Munkelwitz (1994) using EDB and that predicted from thermodynamics (Clegg et al., 1998). Deliquescence and efflorescence transitions were observed at 80% RH and 37–41% RH, respectively, in good agreement with previous studies (Martin, 2000).

Figure 3 shows the changes in (a) peak position and (b) FWHM of  $\nu_1\text{-SO}_4^{2-}$  band in dehydration and hydration processes. In the dehydration process, there was only a slight red shift and broadening of  $\nu_1\text{-SO}_4^{2-}$  until 37% RH, at which point  $\nu_1\text{-SO}_4^{2-}$  shifted sharply from  $978\text{ cm}^{-1}$  to  $975\text{ cm}^{-1}$ , and its FWHM suddenly decreased from  $11\text{ cm}^{-1}$  to  $6\text{ cm}^{-1}$ , corresponding to the efflorescence transition. In the hydrating process, an abrupt blue shift and broadening of the  $\nu_1\text{-SO}_4^{2-}$  band were evident at 80% RH, corresponding to the deliquescence transition. The concurrence of phase transitions and distinct changes in the peak position and FWHM of  $\nu_1\text{-SO}_4^{2-}$  at the same RH indicate that the phase transition can also be identified from the sharp shift of peak position and FWHM of the anion band using Raman spectra. Apparently, the sharp shift of peak position and the sudden change in FWHM of Raman spectra provide a very clear identification of the phase transition.

#### 3.2 The hygroscopic properties of $\text{Ca}(\text{NO}_3)_2$ particles

Figure 4 shows the WSR of  $\text{Ca}(\text{NO}_3)_2$  particles and  $\text{Ca}(\text{NO}_3)_2/\text{CaCO}_3$  particles as a function of RH during dehydration and hydration process. In dehydration process

## Hygroscopic properties of $\text{Ca}(\text{NO}_3)_2$ particles by Raman spectra

Y. J. Liu et al.

Title Page

Abstract

Introduction

Conclusions

References

Tables

Figures

⏪

⏩

◀

▶

Back

Close

Full Screen / Esc

Printer-friendly Version

Interactive Discussion

---

**Hygroscopic properties of  $\text{Ca}(\text{NO}_3)_2$  particles by Raman spectra**Y. J. Liu et al.

---

[Title Page](#)[Abstract](#)[Introduction](#)[Conclusions](#)[References](#)[Tables](#)[Figures](#)[◀](#)[▶](#)[◀](#)[▶](#)[Back](#)[Close](#)[Full Screen / Esc](#)[Printer-friendly Version](#)[Interactive Discussion](#)

the  $\text{Ca}(\text{NO}_3)_2$  droplets evaporated following the predicted curve derived from isopiestic measurements with bulk solution (Stokes and Robinson, 1948) above 11% RH. Greater decreases in WSR were observed when RH was decreased from 11% to 7%. Below 7% RH, the WSR was stable at  $\sim 1$  without further significant changes. It indicated that efflorescence occurred at 11–7% RH. Nevertheless, calcium nitrate particles have very low water content under conditions of low humidity and hence low signal-to-noise ratio of the water envelope in Raman spectra. In addition, the calibration curve is extrapolated to high concentration. Thus, the sensitivity and accuracy of the calculated WSR under conditions of low humidity are limited. Therefore, it is not possible to conclude whether a phase transition occurs based solely on changes in water content.

Figure 5 presents microscopic images of a typical calcium nitrate particle in dehydration process. As shown in Fig. 5, the  $\text{Ca}(\text{NO}_3)_2$  droplets changed in size with decreasing RH, but kept spherical shape during the whole dehydration process, even at a RH near to zero. No crystallization was observed, this could be due to the reason that efflorescence was not occurred and  $\text{Ca}(\text{NO}_3)_2$  particles were in a state of highly supersaturated solutions at RH lower than 7%; or a phase transition occurs, e.g. the  $\text{Ca}(\text{NO}_3)_2$  droplets had transformed to amorphous solid particles, which have a spherical shape as the supersaturated  $\text{Ca}(\text{NO}_3)_2$  droplets.

To find out what happened to  $\text{Ca}(\text{NO}_3)_2$  droplets during the dehydration process, especially at RH lower than that of the likely efflorescence point, we investigated the changes in position and FWHM of the  $\nu_1\text{-NO}_3^-$  band in the dehydration process (Fig. 6), because the symmetric stretching vibration band  $\nu_1\text{-NO}_3^-$  is sensitive to structural changes in nitrate solution (Frost and James, 1982; James et al., 1982; Koussinsa and Bertin, 1991). As shown in Fig. 6, there are two transition points in both the curves of peak position vs. RH and that of FWHM vs. RH, i.e. 10% RH and 7% RH. Above 10% RH,  $\nu_1\text{-NO}_3^-$  gradually became broader with decreasing RH and shifted to a higher frequency, from  $1049\text{ cm}^{-1}$  at 70% RH to  $1053\text{ cm}^{-1}$  at 10% RH. From 10% RH to 7% RH,  $\nu_1\text{-NO}_3^-$  showed a much more marked shift to a higher frequency, from  $1053\text{ cm}^{-1}$  to  $1056\text{ cm}^{-1}$ . At the same time, its FWHM showed a slight reduction instead of increasing further.

**Hygroscopic properties of  $\text{Ca}(\text{NO}_3)_2$  particles by Raman spectra**

Y. J. Liu et al.

Title Page

Abstract

Introduction

Conclusions

References

Tables

Figures

⏪

⏩

◀

▶

Back

Close

Full Screen / Esc

Printer-friendly Version

Interactive Discussion

Below 7% RH, both the position and FWHM of the  $\nu_1\text{-NO}_3^-$  band remained unchanged. Concomitant with WSR evolution in the dehydration process, the jump in the  $\nu_1\text{-NO}_3^-$  band position and FWHM at 10–7% RH and lack of further changes below 7% RH provided strong evidence that a different phase occurred below 7% RH and that the transition from solution to this phase occurred at 10–7% RH.

According to band component analysis (Koussinsa and Bertin, 1991), four solvated species were resolved in the  $\nu_1\text{-NO}_3^-$  of  $\text{Ca}(\text{NO}_3)_2$  solution and assigned as free aquated ions  $\text{NO}_3^-(\text{aq})$  at  $1047.6\text{ cm}^{-1}$ , solvent-separated ion pairs  $\text{NO}_3^-\cdot\text{H}_2\text{O}\cdot\text{Ca}^{2+}$  at  $1050\text{ cm}^{-1}$ , contact ion pairs  $\text{NO}_3^-\cdot\text{Ca}^{2+}$  at  $1053\text{ cm}^{-1}$ , and ion aggregates  $(\text{NO}_3^-\cdot\text{Ca}^{2+})_x$  at  $1055\text{ cm}^{-1}$ . The gradual blue shift of  $\nu_1\text{-NO}_3^-$  from  $1049\text{ cm}^{-1}$  at 70% RH to  $1053\text{ cm}^{-1}$  at 10% RH (Fig. 6a) corresponds to an increasing proportion of more ordered species such as contact ion pairs and ion aggregates in supersaturated solutions. Because the most ordered species  $(\text{NO}_3^-\cdot\text{Ca}^{2+})_x$  in calcium nitrate solution appeared at  $1055\text{ cm}^{-1}$ , whereas that of anhydrate nitrate appeared at  $1067\text{ cm}^{-1}$  (Tang and Fung, 1997), the band maximized at  $1056\text{ cm}^{-1}$  below 7% RH is indicative of a phase between these species. In addition, the narrower band width below 10% RH is an indication of nitrate ions with more fixed orientations in microenvironments than in corresponding supersaturated solution (Zhang et al., 2004). Based on the Raman spectroscopic analysis and the microscopic observation of morphology, we are confident that during the dehydration process,  $\text{Ca}(\text{NO}_3)_2$  droplets had transformed to amorphous hydrate particles at 10–7% RH.

In the hydration process, the amorphous  $\text{Ca}(\text{NO}_3)_2$  remained unchanged until ~7% RH, at which point its water content began to increase and the  $\nu_1\text{-NO}_3^-$  shifted to a lower frequency with increasing FWHM. Above 10% RH, both the growth of the WSR and the red shift of the  $\nu_1\text{-NO}_3^-$  slowed down, and remarkably, the FWHM of the  $\nu_1\text{-NO}_3^-$  begin to decrease. These observations indicate that deliquescence of amorphous  $\text{Ca}(\text{NO}_3)_2$  began at ~7% RH and transformed to solution droplets above 10% RH. Both the curve of WSR vs. RH (Fig. 5) and the curves of peak position and FWHM

of  $\nu_1\text{-NO}_3^-$  vs. RH (Fig. 6) in the hydration process showed excellent agreement to those in the dehydration process, indicating that the deliquescence and efflorescence of amorphous calcium nitrate are reversible processes.

### 3.3 Hygroscopic properties of internally mixed $\text{Ca}(\text{NO}_3)_2/\text{CaCO}_3$ particles

Although field results of completely processed  $\text{CaCO}_3$  particles have been reported,  $\text{Ca}(\text{NO}_3)_2$  and carbonate mineral components are internally mixed in most cases (Mamane and Gottlieb, 1992; Ro et al., 2002, 2005; Shi et al., 2008). To understand the hygroscopic properties of  $\text{Ca}(\text{NO}_3)_2$ -containing mineral dust particles, internally mixed  $\text{Ca}(\text{NO}_3)_2/\text{CaCO}_3$  particles were prepared by exposing individual  $\text{CaCO}_3$  particles to the  $\text{NO}_2/\text{H}_2\text{O}/\text{N}_2$  mixture, and their hygroscopic behavior was studied. The  $\text{CaCO}_3$  particle was present in irregular crystalline form before the exposure to  $\text{NO}_2/\text{H}_2\text{O}/\text{N}_2$  mixture (Fig. 7a). The reacted  $\text{CaCO}_3$  particle clearly increased in size and become round, with two distinctly different parts (Fig. 7b). Raman mapping results further confirmed that this was a  $\text{Ca}(\text{NO}_3)_2$  solution shell surrounding a  $\text{CaCO}_3$  crystalline core (Fig. 7c).

Changes in the water content of the internally mixed  $\text{Ca}(\text{NO}_3)_2/\text{CaCO}_3$  particles in hydration and dehydration processes are presented in Fig. 4. The particle water content was quantified using a method identical to that used for pure  $\text{Ca}(\text{NO}_3)_2$  particles, denoted as the water-to- $\text{Ca}(\text{NO}_3)_2$  molar ratio. The corresponding evolution of  $\nu_1\text{-NO}_3^-$  band position and FWHM is also illustrated in Fig. 6a and b. From Figs. 4 and 6, we can easily see that the internally mixed  $\text{Ca}(\text{NO}_3)_2/\text{CaCO}_3$  particles exhibit hygroscopic behavior identical to that of pure  $\text{Ca}(\text{NO}_3)_2$  particles in both hydration and dehydration processes. Their  $\text{Ca}(\text{NO}_3)_2$  shell is in the amorphous hydrate state below 7% RH, and both deliquescence and efflorescence transition occur at 7–10% RH. Once in solution, the particles grow and evaporate following the curve derived from isopiestic measurements with bulk solution of calcium nitrate. In conclusion, the hygroscopic behavior of internally mixed  $\text{Ca}(\text{NO}_3)_2/\text{CaCO}_3$  particles is determined by the  $\text{Ca}(\text{NO}_3)_2$ . The slightly soluble  $\text{CaCO}_3$  core has a negligible effect on the phase transition and RH

## Hygroscopic properties of $\text{Ca}(\text{NO}_3)_2$ particles by Raman spectra

Y. J. Liu et al.

Title Page

Abstract

Introduction

Conclusions

References

Tables

Figures

◀

▶

◀

▶

Back

Close

Full Screen / Esc

Printer-friendly Version

Interactive Discussion



dependence of the particle water content.

## 4 Discussion

Compared with EDB, ESEM, and TDMA, micro-Raman spectrometry provides more than one way to investigate the hygroscopic behavior of calcium nitrate particles. The water content can be quantified by the relative intensity of Raman bands, the morphological changes can be observed with microscope equipped to Raman spectrometer, and at the same time, the  $\nu_1$ -NO<sub>3</sub><sup>-</sup> band position and FWHM are sensitive to structural changes. Although the RH dependence of particle water content and morphological changes are expressions of hygroscopic properties, chemical structural changes are actually the determining factor. This factor is complementary and can help to gain a more complete understanding of the hygroscopic process. As described in Sect. 3, evidence of a phase transition was found in the curve of water content vs. RH and, more importantly and obviously, in the curve of the  $\nu_1$ -NO<sub>3</sub><sup>-</sup> band position and width vs. RH. Moreover, based on the results of the  $\nu_1$ -NO<sub>3</sub><sup>-</sup> band analysis, we can confirm with high confidence that the new phase is an amorphous solid.

Raman spectrometry is a promising technique for quantifying the water content of droplets that have insoluble inclusions. The most commonly used techniques to measure particle water content are EDB and TDMA, which measure the total mass and size of particles, respectively. However, if insoluble inclusions are present in a droplet, the water content or concentration of the droplet cannot be determined by EDB or TDMA if the precise mass or size of the inclusion is unknown. In contrast, the presence of inclusions will not affect the quantification of droplet concentration with Raman spectrometry because the water content is determined directly using the relative intensity of the solute Raman band to water Raman band. In the case of internally mixed Ca(NO<sub>3</sub>)<sub>2</sub>/CaCO<sub>3</sub> particles, the WSR was quantified accurately even when the ratio of Ca(NO<sub>3</sub>)<sub>2</sub> to CaCO<sub>3</sub> was unknown. In the atmosphere, soluble salts or organic components are often internally mixed with insoluble soot or mineral components (Posfai et al.,

### Hygroscopic properties of Ca(NO<sub>3</sub>)<sub>2</sub> particles by Raman spectra

Y. J. Liu et al.

Title Page

Abstract

Introduction

Conclusions

References

Tables

Figures

⏪

⏩

◀

▶

Back

Close

Full Screen / Esc

Printer-friendly Version

Interactive Discussion



1999; Vogt et al., 2003; Ro et al., 2002, 2005). Our knowledge of the physicochemical properties of these complicated aerosol particles is far from complete. Raman spectrometry may be a very useful tool with which to investigate the hygroscopic behaviors of these complicated aerosol particles.

5 The deliquescence process of amorphous  $\text{Ca}(\text{NO}_3)_2$  particles demonstrated here can explain the morphological changes observed by ESEM (Laskin et al., 2005b) and agree with the deliquescence transition point identified by TDMA (Gibson et al., 2006). However, our findings differ from those obtained by EDB (Tang and Fung, 1997), which showed a higher deliquescence RH of  $\sim 13\%$  RH. The EDB results also indicated a different dehydration process that  $\text{Ca}(\text{NO}_3)_2$  droplets continued to lose water upon system  
10 evacuation until in vacuum (0% RH) they turned into amorphous solid particles with a WSR of 1:1. In contrast, in our study the changes in water content and in  $\nu_1\text{-NO}_3^-$  band position and FWHM both indicated that the efflorescence transition occurred at 10–7% RH. Although there have been no other reports regarding the calcium nitrate dehydra-  
15 tion process, Gibson et al. (2006) prepared amorphous calcium nitrate for hydration experiments by evaporating droplets in a diffusion dryer in which the RH can be reduced to only several percent; their findings support our observation that efflorescence occurs above 0% RH.

The disagreement between our results and those reported by Tang and Fung (1997)  
20 may have been because of the different equilibrium time used. The gas transport in very viscous particles can hinder gas–particle equilibrium. For example, Chan et al. (2000) reported significant retardation of the water evaporation rate of highly concentrated  $\text{Mg}(\text{SO}_4)_2$  droplets. We performed pre-experiments to ensure that equilibrium could be reached at each RH. It took approximately 15 min for a  $\text{Ca}(\text{NO}_3)_2$  particle with several micrometers in diameter to attain an equilibrium state at 7–10% RH.  
25 However, the equilibrium time that is normally used in hygroscopic experiments is on the order of a few seconds (Chan and Chan, 2005), which is too short for sufficient mass transfer for viscous supersaturated  $\text{Ca}(\text{NO}_3)_2$  droplets. The equilibrium time was not explicitly stated by Tang and Fung's paper, if inadequate equilibrium time was used

---

## Hygroscopic properties of $\text{Ca}(\text{NO}_3)_2$ particles by Raman spectra

Y. J. Liu et al.

---

[Title Page](#)[Abstract](#)[Introduction](#)[Conclusions](#)[References](#)[Tables](#)[Figures](#)[⏪](#)[⏩](#)[◀](#)[▶](#)[Back](#)[Close](#)[Full Screen / Esc](#)[Printer-friendly Version](#)[Interactive Discussion](#)

in their experiment, the observed RHs of efflorescence and deliquescence would have been underestimated and overestimated, respectively.

Crystallographic studies indicate that anhydrate calcium nitrate and its di-, tri-, and tetrahydrates occur as solid phases (Frazier et al., 1964). The corresponding stable form in different ranges of RH has been predicted by bulk thermodynamics (Kelly and Wexler, 2005). The tetrahydrate is expected to be in the solid phase in equilibrium with the  $\text{Ca}(\text{NO}_3)_2$  saturated solution with a transition point at 50% RH (Fig. 4). Solid–solid phase transitions are expected below 50% RH, including transformation from tetrahydrate to trihydrate at 17% RH, from trihydrate to dehydrate at 11% RH, and from dehydrate to anhydrate at 9% RH. However, instead of transforming into the tetrahydrate at 50% RH as expected,  $\text{Ca}(\text{NO}_3)_2$  droplets continuously lost water until they were highly supersaturated at 10% RH, after which they began to convert to a solid metastable phase, i.e. amorphous hydrate, which was not predicted by bulk thermodynamics. Hysteresis of efflorescence is very common for microparticles and is usually explained by the absence of heterogeneous nucleation (Martin, 2000). However, kinetic limitations cannot explain the hygroscopic behavior of  $\text{Ca}(\text{NO}_3)_2$  particles completely. As shown in Sect. 3, the internally mixed  $\text{Ca}(\text{NO}_3)_2/\text{CaCO}_3$  particles effloresce at the same relative humidity as pure  $\text{Ca}(\text{NO}_3)_2$  particles, although there are large  $\text{CaCO}_3$  nuclei in these particles that can invariably induce heterogeneous nucleation. Further investigations are required to determine why the calcium nitrate solution shell on dust particles does not transform to its stable tetrahydrate. Nevertheless, these observations indicate the very different behavior and mechanism of phase transition in microparticles than those in bulk samples. In another word, it is inappropriate to infer the phase transition behavior of  $\text{Ca}(\text{NO}_3)_2$  microparticles from their bulk properties.

In fact, in addition to the very different properties of calcium nitrate particles as compared with bulk samples, Tang et al. (1995) also reported discrepancies between microparticle hygroscopic behavior and bulk thermodynamic predictions for some other salts. The role of atmospheric aerosol particles, therefore, cannot always be assessed solely based on bulk properties. Care should be taken when using bulk thermodynamic

## Hygroscopic properties of $\text{Ca}(\text{NO}_3)_2$ particles by Raman spectra

Y. J. Liu et al.

Title Page

Abstract

Introduction

Conclusions

References

Tables

Figures

⏪

⏩

◀

▶

Back

Close

Full Screen / Esc

Printer-friendly Version

Interactive Discussion

calculations to infer aerosol properties; some experiments for the study of aerosol properties using bulk samples may lead to erroneous results.

## 5 Conclusions and atmospheric implications

Our results indicate that the micro-Raman technique is a powerful tool with which to investigate the hygroscopic behavior of individual  $\text{Ca}(\text{NO}_3)_2$  and internally mixed  $\text{Ca}(\text{NO}_3)_2/\text{CaCO}_3$  particles. The RH dependence of the water content was quantified accurately for  $\text{Ca}(\text{NO}_3)_2$  particles with and without  $\text{CaCO}_3$  inclusion. Significant new spectroscopic evidence related to chemical structure was provided to identify phase transitions and to determine phases. Thus, the hygroscopic behavior of  $\text{Ca}(\text{NO}_3)_2$  particles was characterized in more detail and more reliably than had been possible previously, and the hygroscopic properties of internally mixed  $\text{Ca}(\text{NO}_3)_2/\text{CaCO}_3$  particles were investigated systematically for the first time.

The deliquescence and efflorescence of individual  $\text{Ca}(\text{NO}_3)_2$  particles were reversible processes. The  $\text{Ca}(\text{NO}_3)_2$  particles were in the form of solution droplets above 10% RH and amorphous hydrates below 7% RH; phase transitions occurred between 7–10% RH. The hygroscopic behavior of internally mixed  $\text{Ca}(\text{NO}_3)_2/\text{CaCO}_3$  particles was fully controlled by the  $\text{Ca}(\text{NO}_3)_2$  and was identical to that of pure  $\text{Ca}(\text{NO}_3)_2$  particles. That is, the slightly soluble  $\text{CaCO}_3$  core has a negligible effect on phase transition and the RH dependence of the particle water content.

Typical ambient relative humidity is in the range of 20–90%; thus, calcium nitrate particles or calcium nitrate products on mineral dust particles are usually in the solution state in the atmosphere, whereas the original mineral particles are normally insoluble. The formation of calcium nitrate on dust particles can therefore markedly change its water content and hygroscopic properties. Its impact on radiation and climate has been discussed extensively (Vlasenko et al., 2006; Prince et al., 2007; Gibson et al., 2006). Here, we would like to emphasize its effect on the reactivity of mineral dust. The strong hygroscopic properties of calcium nitrate product make the heterogeneous re-

### Hygroscopic properties of $\text{Ca}(\text{NO}_3)_2$ particles by Raman spectra

Y. J. Liu et al.

Title Page

Abstract

Introduction

Conclusions

References

Tables

Figures

⏪

⏩

◀

▶

Back

Close

Full Screen / Esc

Printer-friendly Version

Interactive Discussion

actions of mineral dust with reactive nitrogen species unlimited to the particle surface. This was supported by the results of laboratory and field studies of completely processed calcium carbonate dust particles (Laskin et al., 2005a; Krueger et al., 2003). Once a calcium nitrate solution film has formed, the interface where the heterogeneous reaction takes place will change from gas–solid to gas–solution–solid. Consequently, the reaction mechanism will be completely different, and mass transfer in the solution layer should also be considered.

## Appendix A

### Calibration curves of $(\text{NH}_4)_2\text{SO}_4$ and $\text{Ca}(\text{NO}_3)_2$

See Fig. A1.

*Acknowledgements.* This work was supported by the National Basic Research Priorities Program (Grant No. 2002CB410802) and National Natural Science Foundation of China (Grant No. 40490265).

## References

- Chan, C. K., Choi, M. Y., and Zhang, Y.: Observation of mass transfer limitation in evaporation of single levitated droplets, *J. Aerosol Sci.*, 31, 989–990, 2000.
- Chan, M. N. and Chan, C. K.: Mass transfer effects in hygroscopic measurements of aerosol particles, *Atmos. Chem. Phys.*, 5, 2703–2712, 2005,  
<http://www.atmos-chem-phys.net/5/2703/2005/>.
- Chen, Q., Zhu, T., Li, H., Ding, J., and Li, Y.: In-situ investigation of the heterogeneous reactions on atmospheric particles by micro-Raman spectrometry, *Prog. Nat. Sci.*, 15, 1518–1522, 2005.
- Clegg, S. L., Brimblecombe, P., and Wexler, A. S.: Thermodynamic model of the system  $\text{H}^+ - \text{NH}_4^+ - \text{SO}_4^{2-} - \text{NO}_3^- - \text{H}_2\text{O}$  at tropospheric temperatures, *J. Phys. Chem. A*, 102, 2137–2154, 1998.

## Hygroscopic properties of $\text{Ca}(\text{NO}_3)_2$ particles by Raman spectra

Y. J. Liu et al.

Title Page

Abstract

Introduction

Conclusions

References

Tables

Figures

⏪

⏩

◀

▶

Back

Close

Full Screen / Esc

Printer-friendly Version

Interactive Discussion

---

**Hygroscopic  
properties of  
Ca(NO<sub>3</sub>)<sub>2</sub> particles by  
Raman spectra**Y. J. Liu et al.

---

[Title Page](#)[Abstract](#)[Introduction](#)[Conclusions](#)[References](#)[Tables](#)[Figures](#)[⏪](#)[⏩](#)[◀](#)[▶](#)[Back](#)[Close](#)[Full Screen / Esc](#)[Printer-friendly Version](#)[Interactive Discussion](#)

Dentener, F. J., Carmichael, G. R., Zhang, Y., Lelieveld, J., and Crutzen, P. J.: Role of mineral aerosol as a reactive surface in the global troposphere, *J. Geophys. Res. Atmos.*, 101, 22 869–22 889, 1996.

Frazier, A. W., Mullins, R. C., and Smith, J. P.: Fertilizer Materials, *Crystallography of Hydrates of Calcium Nitrate*, *J. Agric. Food Chem.*, 12, 478–479, 1964.

Frost, R. L. and James, D. W.: Ion Ion Solvent Interactions in Solution .3. Aqueous-Solutions of Sodium-Nitrate, *J. Chem. Soc., Faraday Trans. 1*, 78, 3223–3234, 1982.

Gibson, E. R., Hudson, P. K., and Grassian, V. H.: Physicochemical properties of nitrate aerosols: Implications for the atmosphere, *J. Phys. Chem. A*, 110, 11 785–11 799, 2006.

Godoi, R. H. M., Potgieter-Vermaak, S., De Hoog, J., Kaegi, R., and Grieken, R.: Substrate selection for optimum qualitative and quantitative single atmospheric particles analysis using nano-manipulation, sequential thin-window electron probe X-ray microanalysis and micro-Raman spectrometry, *Spectrochim. Acta B Atom. Spectros.*, 61, 375–388, 2006.

Hannon, M. J., Boerio, F. J., and Koenig, J. L.: Vibrational Analysis of Polytetrafluoroethylene, *J. Chem. Phys.*, 50, 2829–2836, 1969.

James, D. W., Carrick, M. T., and Frost, R. L.: Structure of Aqueous-Solutions – Fourier Transformation and Band Component Analysis in Magnesium-Nitrate Solutions, *J. Raman Spectrosc.*, 13, 115–119, 1982.

Jordanov, N. and Zellner, R.: Investigations of the hygroscopic properties of ammonium sulfate and mixed ammonium sulfate and glutaric acid micro droplets by means of optical levitation and Raman spectroscopy, *Phys. Chem. Chem. Phys.*, 8, 2759–2764, 2006.

Kelly, J. T. and Wexler, A. S.: Thermodynamics of carbonates and hydrates related to heterogeneous reactions involving mineral aerosol, *J. Geophys. Res.*, 110, D11201, doi:10.1029/2004JD005583, 2005.

Koussinsa, F. and Bertin, F.: Raman Microspectrometric Study of the Dissolution Layer of M(NO<sub>3</sub>)<sub>2</sub>·nH<sub>2</sub>O Crystals (M = Mg, Ca, Zn and Cd) in Their Undersaturated Aqueous-Solutions, *J. Raman Spectrosc.*, 22, 169–176, 1991.

Krueger, B. J., Grassian, V. H., Laskin, A., and Cowin, J. P.: The transformation of solid atmospheric particles into liquid droplets through heterogeneous chemistry: Laboratory insights into the processing of calcium containing mineral dust aerosol in the troposphere, *Geophys. Res. Lett.*, 30, 1148, doi:10.1029/2002GL016563, 2003.

Krueger, B. J., Grassian, V. H., Cowin, J. P., and Laskin, A.: Heterogeneous chemistry of individual mineral dust particles from different dust source regions: the importance of particle

- mineralogy, *Atmos. Environ.*, 38, 6253–6261, 2004.
- Laskin, A., Iedema, M. J., Ichkovich, A., Graber, E. R., Taraniuk, I., and Rudich, Y.: Direct observation of completely processed calcium carbonate dust particles, *Faraday Discuss.*, 130, 453–468, 2005a.
- 5 Laskin, A., Wietsma, T. W., Krueger, B. J., and Grassian, V. H.: Heterogeneous chemistry of individual mineral dust particles with nitric acid: A combined CCSEM/EDX, ESEM, and ICP-MS study, *J. Geophys. Res. Atmos.*, 110, D10208, doi:10.1029/2004JD005206, 2005b.
- Lee, S. H., Murphy, D. M., Thomson, D. S., and Middlebrook, A. M.: Chemical components of single particles measured with Particle Analysis by Laser Mass Spectrometry (PALMS) during the Atlanta SuperSite Project: Focus on organic/sulfate, lead, soot, and mineral particles, *J. Geophys. Res. Atmos.*, 107, 4003, doi:10.1029/2000JD000011, 2002.
- 10 Mamane, Y. and Gottlieb, J.: Nitrate Formation on Sea-Salt and Mineral Particles – a Single-Particle Approach, *Atmos. Environ. Gen. Top.*, 26, 1763–1769, 1992.
- Martin, S. T.: Phase transitions of aqueous atmospheric particles, *Chem. Rev.*, 100, 3403–3453, 2000.
- 15 Musick, J., Popp, J., and Kiefer, W.: Observation of a phase transition in an electrodynamically levitated  $\text{NH}_4\text{NO}_3$  microparticle by Mie and Raman scattering, *J. Raman Spectrosc.*, 31, 217–219, 2000.
- Parsons, M. T., Mak, J., Lipetz, S. R., and Bertram, A. K.: Deliquescence of malonic, succinic, glutaric, and adipic acid particles, *J. Geophys. Res. Atmos.*, 109, D06212, doi:10.1029/2003JD004075, 2004.
- 20 Posfai, M., Anderson, J. R., Buseck, P. R., and Sievering, H.: Soot and sulfate aerosol particles in the remote marine troposphere, *J. Geophys. Res. Atmos.*, 104, 21 685–21 693, 1999.
- Prince, A. P., Grassian, V. H., Kleiber, P., and Young, M. A.: Heterogeneous conversion of calcite aerosol by nitric acid, *Phys. Chem. Chem. Phys.*, 9, 622–634, 2007.
- 25 Reid, J. P., Meresman, H., Mitchem, L., and Symes, R.: Spectroscopic studies of the size and composition of single aerosol droplets, *Int. Rev. Phys. Chem.*, 26, 139–192, 2007.
- Ro, C. U., Kim, H., Oh, K. Y., Yea, S. K., Lee, C. B., Jang, M., and Grieken, R. V.: Single-particle characterization of urban aerosol particles collected in three Korean cities using low-Z electron probe X-ray microanalysis, *Environ. Sci. Technol.*, 36, 4770–4776, 2002.
- 30 Ro, C. U., Hwang, H., Chun, Y., and Van Grieken, R.: Single-particle characterization of four “Asian Dust” samples collected in Korea, using low-Z particle electron probe X-ray microanalysis, *Environ. Sci. Technol.*, 39, 1409–1419, 2005.

---

## Hygroscopic properties of $\text{Ca}(\text{NO}_3)_2$ particles by Raman spectra

Y. J. Liu et al.

---

[Title Page](#)[Abstract](#)[Introduction](#)[Conclusions](#)[References](#)[Tables](#)[Figures](#)[⏪](#)[⏩](#)[◀](#)[▶](#)[Back](#)[Close](#)[Full Screen / Esc](#)[Printer-friendly Version](#)[Interactive Discussion](#)

---

**Hygroscopic properties of  $\text{Ca}(\text{NO}_3)_2$  particles by Raman spectra**Y. J. Liu et al.

---

[Title Page](#)[Abstract](#)[Introduction](#)[Conclusions](#)[References](#)[Tables](#)[Figures](#)[⏪](#)[⏩](#)[◀](#)[▶](#)[Back](#)[Close](#)[Full Screen / Esc](#)[Printer-friendly Version](#)[Interactive Discussion](#)

- Seinfeld, J. H., Carmichael, G. R., Arimoto, R., Conant, W. C., Brechtel, F. J., Bates, T. S., Cahill, T. A., Clarke, A. D., Doherty, S. J., Flatau, P. J., Huebert, B. J., Kim, J., Markowicz, K. M., Quinn, P. K., Russell, L. M., Russell, P. B., Shimizu, A., Shinzuka, Y., Song, C. H., Tang, Y. H., Uno, I., Vogelmann, A. M., Weber, R. J., Woo, J. H., and Zhang, X. Y.: ACE-ASIA – Regional climatic and atmospheric chemical effects of Asian dust and pollution, *B. Am. Meteorol. Soc.*, 85, 367–380, 2004.
- Shi, Z., Zhang, D., Hayashi, M., Ogata, H., Ji, H., and Fujiie, W.: Influences of sulfate and nitrate on the hygroscopic behaviour of coarse dust particles, *Atmos. Environ.*, 42, 822–827, 2008.
- Song, C. H. and Carmichael, G. R.: A three-dimensional modeling investigation of the evolution processes of dust and sea-salt particles in east Asia, *J. Geophys. Res. Atmos.*, 106, 18 131–18 154, 2001.
- Stokes, R. H. and Robinson, R. A.: *Ionic Hydration and Activity in Electrolyte Solutions*, *J. Am. Chem. Soc.*, 70, 1870–1878, 1948.
- Sullivan, R. C., Guazzotti, S. A., Sodeman, D. A., and Prather, K. A.: Direct observations of the atmospheric processing of Asian mineral dust, *Atmos. Chem. Phys.*, 7, 1213–1236, 2007, <http://www.atmos-chem-phys.net/7/1213/2007/>.
- Tang, I. N. and Munkelwitz, H. R.: Water activities, densities, and refractive indices of aqueous sulfates and sodium nitrate droplets of atmospheric importance, *J. Geophys. Res.*, 99, 18 801–18 808, 1994.
- Tang, I. N., Fung, K. H., Imre, D. G., and Munkelwitz, H. R.: Phase-Transformation and Metastability of Hygroscopic Microparticles, *Aerosol Sci. Tech.*, 23, 443–453, 1995.
- Tang, I. N. and Fung, K. H.: Hydration and Raman scattering studies of levitated microparticles:  $\text{Ba}(\text{NO}_3)_2$ ,  $\text{Sr}(\text{NO}_3)_2$ , and  $\text{Ca}(\text{NO}_3)_2$ , *J. Chem. Phys.*, 106, 1653–1660, 1997.
- Tang, Y. H., Carmichael, G. R., Kurata, G., Uno, I., Weber, R. J., Song, C. H., Guttikunda, S. K., Woo, J. H., Streets, D. G., Wei, C., Clarke, A. D., Huebert, B., and Anderson, T. L.: Impacts of dust on regional tropospheric chemistry during the ACE-Asia experiment: A model study with observations, *J. Geophys. Res. Atmos.*, 109, D19S21, doi:10.1029/2003JD003806, 2004.
- Tegen, I., Lacis, A. A., and Fung, I.: The influence on climate forcing of mineral aerosols from disturbed soils, *Nature*, 380, 419–422, 1996.
- Vlasenko, A., Sjogren, S., Weingartner, E., Stemmler, K., Gaggeler, H. W., and Ammann, M.: Effect of humidity on nitric acid uptake to mineral dust aerosol particles, *Atmos. Chem. Phys.*, 6, 2147–2160, 2006,

<http://www.atmos-chem-phys.net/6/2147/2006/>.

- Vogt, R., Kirchner, U., Scheer, V., Hinz, K. P., Trimborn, A., and Spengler, B.: Identification of diesel exhaust particles at an Autobahn, urban and rural location using single-particle mass spectrometry, *J. Aerosol Sci.*, 34, 319–337, 2003.
- 5 Widmann, J. F., Aardahl, C. L., and Davis, E. J.: Microparticle Raman spectroscopy, *Trac-Trend. Anal. Chem.*, 17, 339–345, 1998.
- Zhang, Y. H., Choi, M. Y., and Chan, C. K.: Relating hygroscopic properties of magnesium nitrate to the formation of contact ion pairs, *J. Phys. Chem. A*, 108, 1712–1718, 2004.

ACPD

8, 10597–10625, 2008

---

**Hygroscopic  
properties of  
 $\text{Ca}(\text{NO}_3)_2$  particles by  
Raman spectra**

Y. J. Liu et al.

---

Title Page

Abstract

Introduction

Conclusions

References

Tables

Figures

⏪

⏩

◀

▶

Back

Close

Full Screen / Esc

Printer-friendly Version

Interactive Discussion

## Hygroscopic properties of $\text{Ca}(\text{NO}_3)_2$ particles by Raman spectra

Y. J. Liu et al.

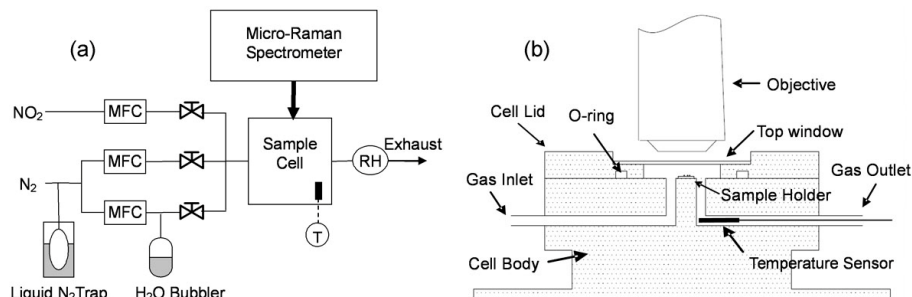


**Fig. 1.** Schematic diagram of the (a) experimental setup and (b) sample cell.

[Title Page](#)[Abstract](#)[Introduction](#)[Conclusions](#)[References](#)[Tables](#)[Figures](#)[◀](#)[▶](#)[◀](#)[▶](#)[Back](#)[Close](#)[Full Screen / Esc](#)[Printer-friendly Version](#)[Interactive Discussion](#)

## Hygroscopic properties of $\text{Ca}(\text{NO}_3)_2$ particles by Raman spectra

Y. J. Liu et al.

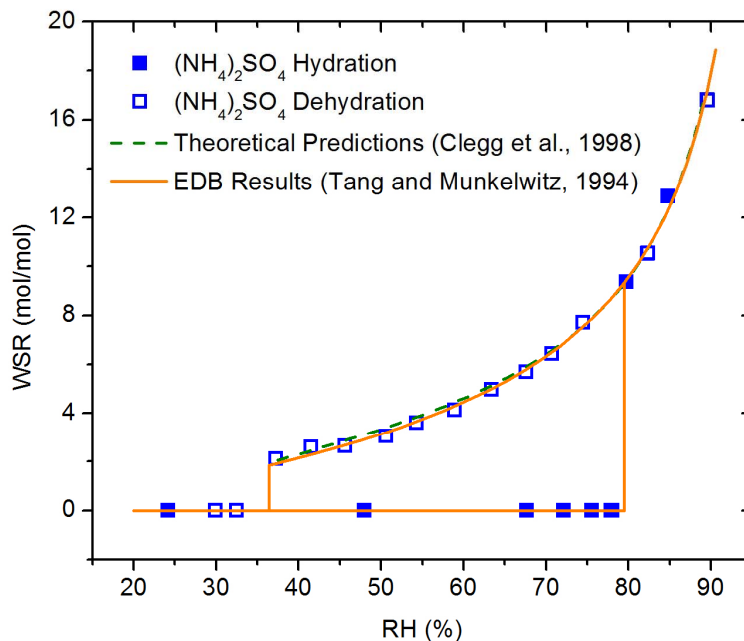


**Fig. 2.** Water-to-solute molar ratio (WSR) of  $(\text{NH}_4)_2\text{SO}_4$  particles as a function of relative humidity (RH) in hydration and dehydration processes.

[Title Page](#)[Abstract](#)[Introduction](#)[Conclusions](#)[References](#)[Tables](#)[Figures](#)[◀](#)[▶](#)[◀](#)[▶](#)[Back](#)[Close](#)[Full Screen / Esc](#)[Printer-friendly Version](#)[Interactive Discussion](#)

## Hygroscopic properties of $\text{Ca}(\text{NO}_3)_2$ particles by Raman spectra

Y. J. Liu et al.

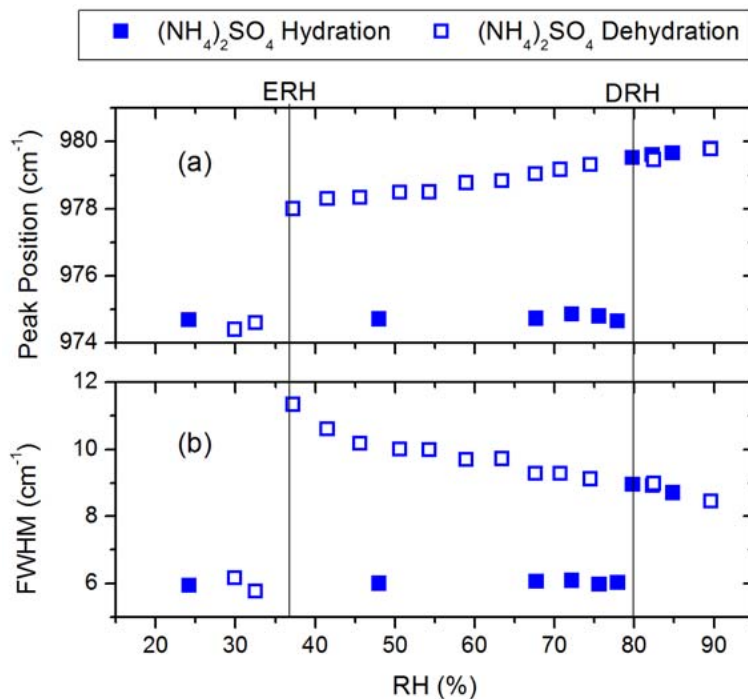


**Fig. 3.** The relative humidity (RH) dependence of **(a)** position and **(b)** full-width at half-maximum (FWHM) of the  $\nu_1\text{-SO}_4^{2-}$  band in hydration and dehydration process.

Title Page

Abstract

Introduction

Conclusions

References

Tables

Figures

◀

▶

◀

▶

Back

Close

Full Screen / Esc

Printer-friendly Version

Interactive Discussion

**Hygroscopic properties of  $\text{Ca}(\text{NO}_3)_2$  particles by Raman spectra**

Y. J. Liu et al.

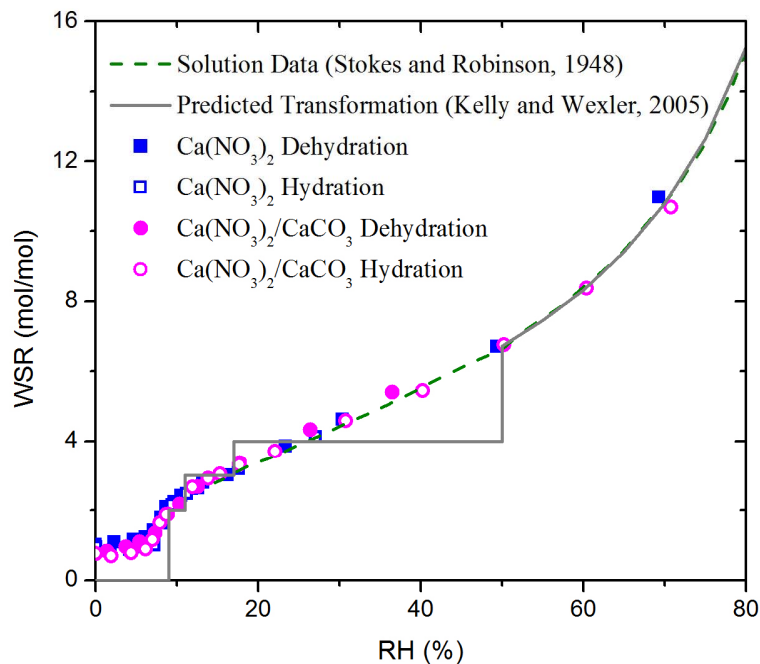


**Fig. 4.** Water-to-solute molar ratio (WSR) of  $\text{Ca}(\text{NO}_3)_2$  and  $\text{Ca}(\text{NO}_3)_2/\text{CaCO}_3$  particles as a function of relative humidity (RH) in dehydration and hydration processes.

[Title Page](#)[Abstract](#)[Introduction](#)[Conclusions](#)[References](#)[Tables](#)[Figures](#)[◀](#)[▶](#)[◀](#)[▶](#)[Back](#)[Close](#)[Full Screen / Esc](#)[Printer-friendly Version](#)[Interactive Discussion](#)

**Hygroscopic properties of  $\text{Ca}(\text{NO}_3)_2$  particles by Raman spectra**

Y. J. Liu et al.

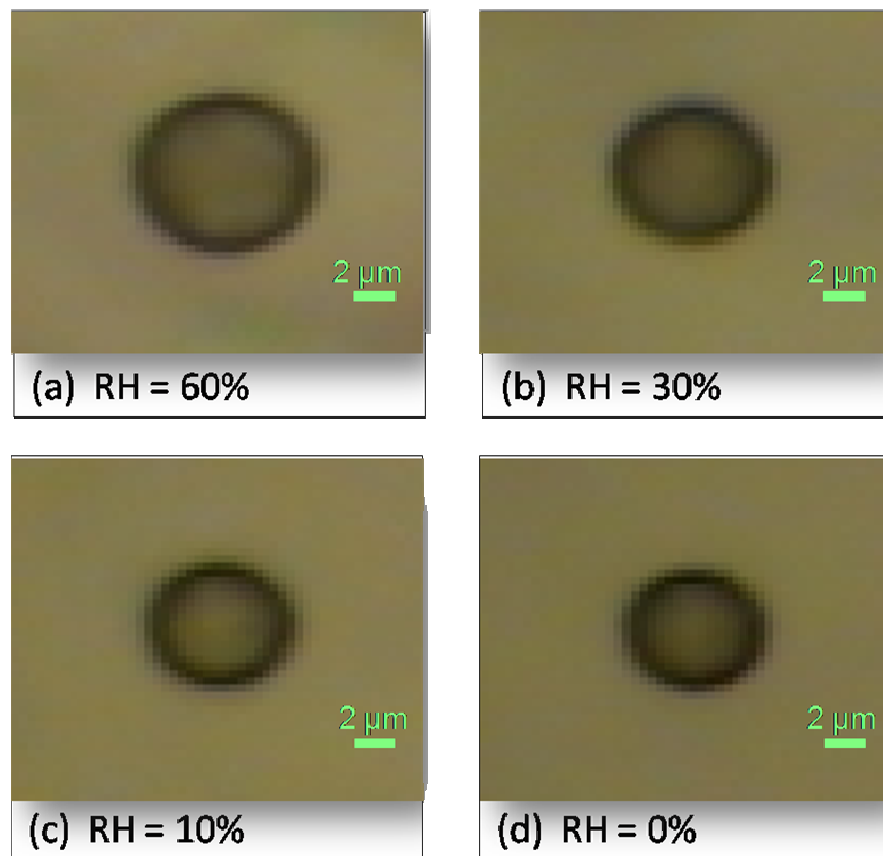


**Fig. 5.** Microscopic images of a typical  $\text{Ca}(\text{NO}_3)_2$  particle in dehydration process.

[Title Page](#)[Abstract](#)[Introduction](#)[Conclusions](#)[References](#)[Tables](#)[Figures](#)[◀](#)[▶](#)[◀](#)[▶](#)[Back](#)[Close](#)[Full Screen / Esc](#)[Printer-friendly Version](#)[Interactive Discussion](#)

Hygroscopic properties of  $\text{Ca}(\text{NO}_3)_2$  particles by Raman spectra

Y. J. Liu et al.

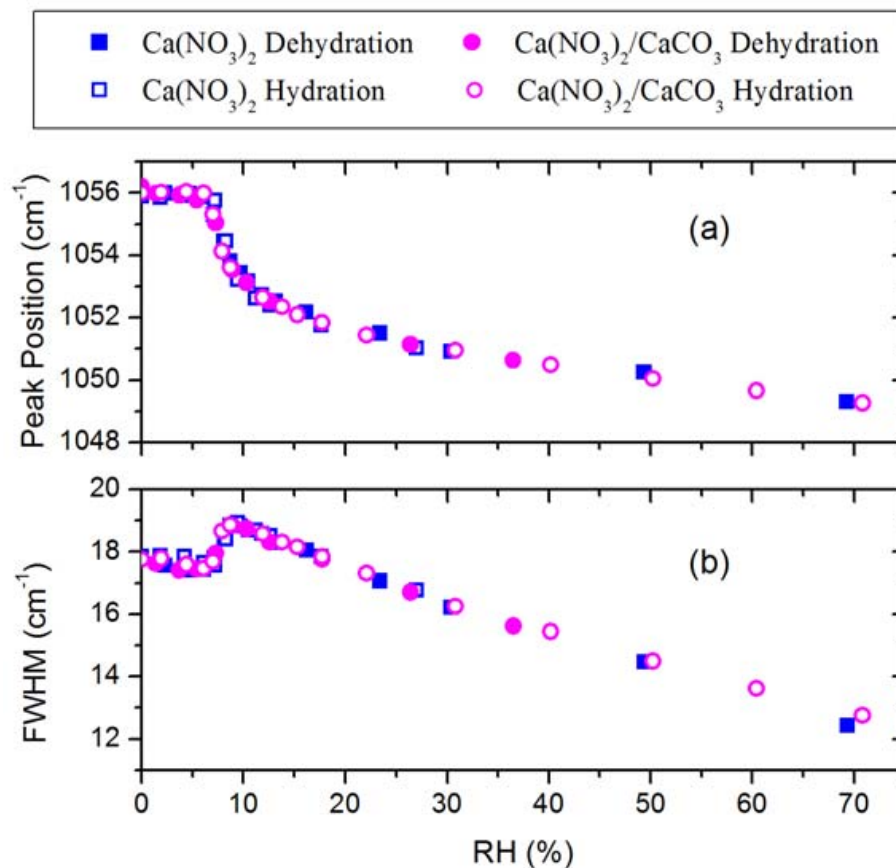


**Fig. 6.** Relative humidity (RH) dependence of **(a)** peak position and **(b)** full width at half-maximum (FWHM) of the  $\nu_1\text{-NO}_3^-$  band of  $\text{Ca}(\text{NO}_3)_2$  and  $\text{Ca}(\text{NO}_3)_2/\text{CaCO}_3$  particles in dehydration and hydration processes.

[Title Page](#)[Abstract](#)[Introduction](#)[Conclusions](#)[References](#)[Tables](#)[Figures](#)[◀](#)[▶](#)[◀](#)[▶](#)[Back](#)[Close](#)[Full Screen / Esc](#)[Printer-friendly Version](#)[Interactive Discussion](#)

## Hygroscopic properties of $\text{Ca}(\text{NO}_3)_2$ particles by Raman spectra

Y. J. Liu et al.

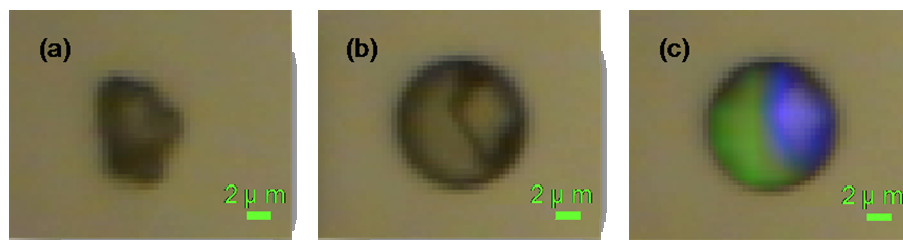


**Fig. 7.** Microscopic images of a typical  $\text{CaCO}_3$  particle **(a)** before and **(b)** after exposure to  $\text{NO}_2$  and **(c)** Raman mapping image after exposure to  $\text{NO}_2$ . The green image represents the average intensity at  $1020\text{--}1075\text{ cm}^{-1}$ , corresponding to  $\nu_1\text{-NO}_3^-$ , whereas the blue image represents the average intensity at  $1075\text{--}1100\text{ cm}^{-1}$ , corresponding to  $\nu_1\text{-CO}_3^{2-}$ .

[Title Page](#)[Abstract](#)[Introduction](#)[Conclusions](#)[References](#)[Tables](#)[Figures](#)[⏪](#)[⏩](#)[◀](#)[▶](#)[Back](#)[Close](#)[Full Screen / Esc](#)[Printer-friendly Version](#)[Interactive Discussion](#)

**Hygroscopic properties of  $\text{Ca}(\text{NO}_3)_2$  particles by Raman spectra**

Y. J. Liu et al.

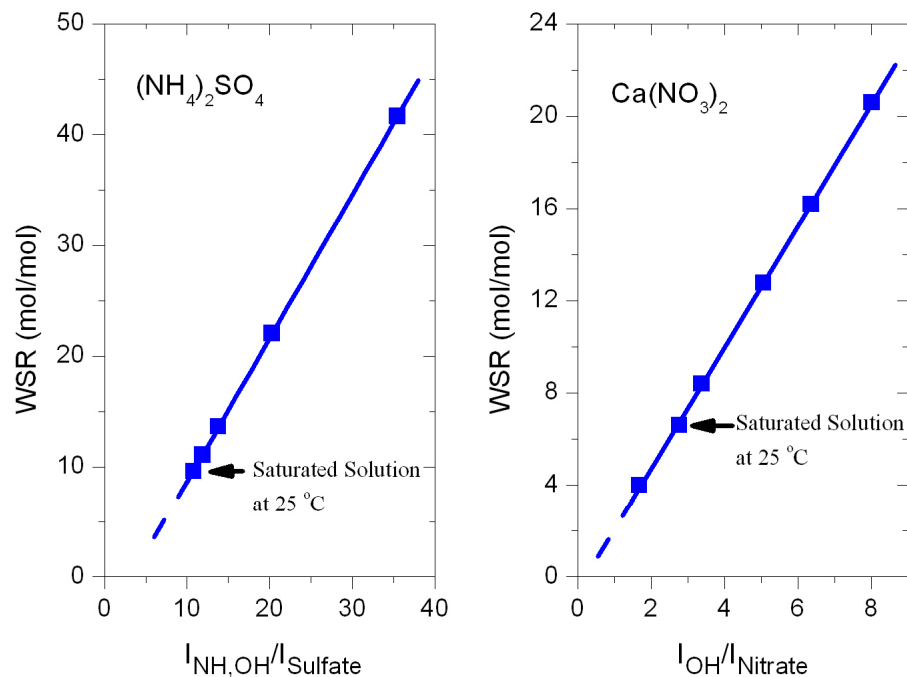


**Fig. A1.** Calibration curves for the water-to-solute molar ratio (WSR) of  $(\text{NH}_4)_2\text{SO}_4$  and  $\text{Ca}(\text{NO}_3)_2$  droplets. The solid line shows the linear fit of the experimental data; the broken line shows the extrapolation to supersaturated concentration.

[Title Page](#)[Abstract](#)[Introduction](#)[Conclusions](#)[References](#)[Tables](#)[Figures](#)[◀](#)[▶](#)[◀](#)[▶](#)[Back](#)[Close](#)[Full Screen / Esc](#)[Printer-friendly Version](#)[Interactive Discussion](#)